

AI-based Radio and Computing Resource Allocation and Path Planning in NOMA NTN: AoI Minimization under CSI Uncertainty

Maryam Ansarifard, Nader Mokari, *Senior Member, IEEE*, Mohammadreza Javan, *Senior Member, IEEE*, Hamid Saeedi, *Senior Member, IEEE*, and Eduard A. Jorswieck, *Fellow, IEEE*

Abstract—In this paper, we develop a hierarchical aerial computing framework composed of high altitude platform (HAP) and unmanned aerial vehicles (UAVs) to compute the fully offloaded tasks of terrestrial mobile users which are connected through an uplink non-orthogonal multiple access (UL-NOMA). To better assess the freshness of information in computation-intensive applications the criterion of age of information (AoI) is considered. In particular, the problem is formulated to minimize the average AoI of users with elastic tasks, by adjusting UAVs' trajectory and resource allocation on both UAVs and HAP, which is restricted by the channel state information (CSI) uncertainty and multiple resource constraints of UAVs and HAP. In order to solve this non-convex optimization problem, two methods of multi-agent deep deterministic policy gradient (MADDPG) and federated reinforcement learning (FRL) are proposed to design the UAVs' trajectory, and obtain channel, power, and CPU allocations. It is shown that task scheduling significantly reduces the average AoI. This improvement is more pronounced for larger task sizes. On one hand, it is shown that power allocation has a marginal effect on the average AoI compared to using full transmission power for all users. Compared with traditional transmission schemes, the simulation results show our scheduling scheme results in a substantial improvement in average AoI.

Index Terms—Age of information (AoI), non-terrestrial networks (NTNs), CSI uncertainty, non-orthogonal multiple access (NOMA).

I. INTRODUCTION

A. State-of-the-Art

In the next generation of wireless networks, developing various traffic types and use cases requires a greater degree of planning and flexibility. As a result of their strong growth in the coming years, internet of things environments (IoT) are the top priorities of these requirements, ranging from machine-type communications to ultra-reliable and low-latency communications, industrial scenarios, and novel applications requiring high throughput. A new cellular IoT technology characterizing reduced-capability (RedCap) user equipments for the fifth-generation (5G) new radio (NR) is introduced in the 3rd generation partnership project (3GPP) Rel-17, which specifies the device capabilities required to support novel mid-end IoT

use cases, including urban monitoring or video surveillance, wearable and industrial wireless sensors [1], [2]. As several services require real-time uplink (UL) data transmission, meeting the stringent requirements of the above industrial applications prompts new solutions in terms of offloading Redcap devices' computation-intensive tasks. Non-terrestrial networks (NTNs), with using elements such as unmanned aerial vehicles (UAVs), high altitude platforms (HAPs), and satellites provide a 3D flexible coverage. Moreover, as the devices on the ground are unable to perform computationally-expensive operations, HAPs and UAVs, equipped with computation resources, are considered as potential candidates for mobile edge computing (MEC) [3]. A fixed HAP remains at an altitude of around 20km equipped with powerful loading equipment such as computing devices, which provides huge coverage, making it an ideal base station in the air. However, terrestrial devices with limited power supplies cannot be connected directly to HAPs. Such a connection can be made through UAVs. Due to their autonomy, flexibility, and wide range of application domains, UAVs have gained popularity over the past few years [4], [5]. To enhance the coverage and communication quality, UAVs are employed as mobile base stations [6], [7]. Also, in order to reduce the access latency and to improve the communication quality of the UAV networks, non-orthogonal multiple access (NOMA) can be applied to the UAV networks.

The traditional approach of offloading tasks to the NTN, whereby the whole task would be sent at once as long as sufficient resources are available, can result in large transmission latency that degrades users' quality of experience (QoE). Therefore, a time-aware task scheduling considering available radio and computation resources is needed. In addition to performing the computations of the received tasks, the freshness of the information is very crucial in delay-sensitive applications. To measure the performance of data freshness at the receiver side, a new metric, called age of information (AoI), is proposed in [8], which is defined as the amount of time elapsed since the freshest delivered update takes place. Many recent works have focused on minimizing this metric in different networks [9], [10]. However, there are some factors that affect this metric, in particular, imperfect channel state information (CSI) resulting from estimation errors and limited feedback from users in practice [11]. Consequently, it is pertinent to take into account the imperfection of CSI in links between ground users and UAVs.

In uncertain environments where the CSI is not perfectly

M. Ansarifard, N. Mokari and H. Saeedi are with the Department of Electrical and Computer Engineering, Tarbiat Modares University, Tehran, Iran, (emails: m.ansarifard, nader.mokari, hsaeeedi@modares.ac.ir). H. Saeedi is also with University of Doha for Science and Technology, Doha, Qatar. M. R. Javan is with the Department of Electrical Engineering, Shahrood University of Technology, Iran, (email: javan@shahroodut.ac.ir). Eduard A. Jorswieck is with Institute for Communications Technology, TU Braunschweig, Germany, email: jorswieck@ifn.ing.tu-bs.de.

known and for time-sensitive applications, managing the resources and mobility of non-terrestrial platforms is a challenging task. Conventional mathematical optimization approaches may fail to converge within the desired time range for these problems, which are usually non-convex [12]. Artificial intelligence (AI) and in particular reinforcement learning (RL) algorithms have been developed in NTN-aided wireless communications and cellular-connected NTNs over the last few years, where by continuously interacting with the environment, the agent will learn a certain skill by using the reward value provided by the environment. The concept of RL has been extensively studied and applied, and it is considered to be one of the core technologies of intelligent systems design. Due to federated learning (FL) success in supervised learning tasks, federated RL (FRL) has become an attractive subject. Using FL, raw data generated locally can be used to train a local model, and then the local model parameters can be used to update the weights of the global model or other local models (in peer-to-peer approach). The multi-agent deep deterministic policy gradient (MADDPG) and FRL can be applied to cooperative, competitive, or mixed multi-agent environments [13]. Although the agent can make decisions and act independently, the environment and other agents will impact its decisions and actions.

This article aims to minimize the average AoI of all ground users in proposed hierarchical NTN architecture, including multi UAVs and a HAP equipped with computational resources to process the received tasks, by elastic task scheduling, radio and computing resource allocation of UAVs and the HAP, and trajectory planning of UAVs. To examine the effect of CSI imperfection, we consider CSI uncertainty in uplink NOMA between ground users and UAVs, and in order to solve this non-convex problem, we adopt MADDPG and FRL approaches.

B. Related Works

UAV-assisted systems have been combined with other technologies such as NOMA. In [14]–[16] NOMA is employed to improve the performance of UAV-enabled communication systems. A swarm of UAVs is considered in [17] to ensure the long-term freshness requirements of situation awareness. To reduce energy consumption under fast-changing environmental dynamics, the authors use a multi-agent deep reinforcement learning (DRL) algorithm with global-local rewards. Based on UAV latency requirements and UAV location, [18] optimizes the total energy consumption of UAVs and users in a multiple UAV-enabled MEC networks planning. Ref. [19] focuses on edge computing for UAVs to track a mobile target and identify it, satisfying stringent latency requirements. Overall cost and inference error have been traded off. On the other hand, HAPs can provide intensive computing services due to their stronger payload. Using a FL-based algorithm, [20] has designed a task computation algorithm for high-altitude computing-enabled balloons to minimize energy and time usage during the data offloading process. The hierarchical aerial computing framework developed by [21], provides MEC services for various IoT applications to maximize total IoT data computed, which is constrained by IoT delays and UAV and HAP resource

requirements. In [22], a deep Q-learning network (DDQN) algorithm is proposed to realize the freshness-aware path planning of the UAV. In IoT systems, AoI-aware UAV-aided wireless network has received significant attention. In [23], the UAV's trajectory and data acquisition mode are optimized in accordance with the aim of minimizing the average AoI of all sensors. Ref. [24] uses the UAV to collect the sensors' data, and the UAV's trajectory is optimized to minimize the average AoI of the system as well as the maximum AoI of the individual wireless sensors. In [25] a trajectory planning strategy for UAVs is proposed to minimize the maximum AoI of a UAV-enabled wireless sensor network, ensuring the well-balanced between the sensors' uploading time and the UAV's flight time. A decentralized computation offloading algorithm is proposed in [26] with the aim of minimizing average task completion time. Ref. [27] minimizes the average AoI of the data collected from all ground sensors by optimizing joint energy transfer and data collection time allocation and UAV's trajectory planning, where the authors decomposed it into two sub-problems and solved it with designing dynamic programming (DP) and ant colony (AC) heuristic algorithms. A distributed optimization problem for resource allocation at the MEC servers is formulated in [28] to maximize the number of offloaded tasks while satisfying heterogeneous quality-of-service (QoS) requirements, and then it is solved using the MADDPG. In [29], the authors propose a heterogeneous multi-agent actor-critic algorithm based on RL to minimize the average AoI in MEC systems. The reality of UAV missions usually involves an uncertain and dynamic environment, so the control architecture must be robust and versatile enough to deal with uncertainty and changes in the environment [30]. Currently, AoI-aware problems have mainly focused on maximizing total data rates of users under perfect CSI. Authors in [31] study the average staleness of CSI in fully connected time-varying reciprocal wireless networks with node equiprobably selected to transmit and distribute CSI in each time slot. In Table I, we have summarized the related works with respect to our proposed framework. As can be seen, in the aforementioned literature, the concentration is on minimizing AoI through UAV trajectory and resource allocation by imposing transmission time constraints. Furthermore, they do not take into account the CSI uncertainty, which is inevitable in the proposed environment. Moreover, Redcap devices' servers have limited computing resources, and this limitation has rarely been paid attention to in these studies. Overall, it appears that AoI-aware scheduling and resource allocation for resource-constrained users and NTN elements remains a challenge. To the best of our knowledge, our work is the first one on minimizing average AoI up to the top layer, i.e., HAP, coupled with CSI imperfection on the user-UAV links, using joint trajectory planning, task scheduling, and resource allocation.

C. Our Contribution

The key contributions of this work are as follows:

- We first formulate the trajectory and resource allocation problem in a NOMA-enabled NTN. The aim of the

TABLE I: Related works comparison.

Ref.	NTN	Resource Allocation	Task Offloading	Task Transmission Method	Trajectory Planning	Uncertainty	Objective Function	Solution
[20]	High altitude balloons (HABs)	✓	✓	Fixed	✗	✗	Minimizing weighted sum of energy and time consumption	SVM-based FL
[21]	UAVs and HAPs	✓	✓	Fixed	✗	✗	Maximizing the total IoT computed data	Game theory, heuristic algorithm
[22]	Single UAV	✓	✓	Fixed	✓	✗	Minimizing average AoI and energy consumption	DDQN
[24]	Single UAV	✗	✓	Fixed	✓	✗	Minimizing max/average AoI	DP, genetic algorithm (GA)
[26]	✗	✗	✓	Fixed	✗	✗	Minimizing average task completion time	MA imitation learning
[27]	Single UAV	✓	✓	Fixed	✓	✗	Minimizing average AoI	DP, AC
[28]	UAV-assisted vehicular network	✓	✓	Fixed	✓	✗	Maximizing the number of offloaded tasks	MADDPG
[29]	Multi-UAVs	✓	✓	Fixed	✓	✗	Minimizing average AoI	MADDPG, EdgeFed
Our work	Both UAVs and HAP	✓	✓	Elastic	✓	✓	Minimizing average AoI	MADDPG, P2P-VFRL

formulated problem is to minimize the average AoI experienced by all the users under CSI uncertainty while satisfying the minimum data rate constraint of users. We notice that the formulated problem is non-convex, and mixed-integer nonlinear problem (MINLP) which cannot be solved globally and efficiently.

- In the existing literature, receiving tasks are constrained by a time limit. This existing scheme is herein referred to as *fixed method*. Due to the low latency and large data volume requirements of RedCap services, the *fixed method* falls short in terms of delivering the whole task, resulting in an increased average AoI. To tackle this issue and to guarantee task timeliness, we propose a novel dynamic task transmission method that, unlike previous studies, does not assume the availability of the required radio and computing resources for the whole task to be offloaded. Our proposed method is compared against the *fixed method* and it is shown that our method performs better in terms of minimizing average AoI.
- In the simulation, we deal with two types of agents, UAV and HAP. They differ in their actions but have the same goal, which is minimizing average AoI. Using online AI-based algorithms, we first present the convergence of the MADDPG approach. Then, we compare the average AoI experienced by the mobile users with a FRL-based algorithm, a peer-to-peer vertical federated reinforcement learning (P2P-VFRL). To the best of our knowledge, this is the first algorithm that combines the peer-to-peer vertical federated (P2P-VF) with the multi-agent actor-critic reinforcement learning, which is dynamically adapted to our problem.

D. Paper Organization

The rest of this paper is organized as follows. The system model and the problem formulation are presented in Section II. In Section III, the solution to the problem is provided. Simulation results are presented in Section IV, and Section V concludes the paper.

Symbol Notations: Column vectors and matrices are denoted by boldface lower case letters and capital letters, respectively. The set of elements is denoted by calligraphic letters. The

transpose of a vector \mathbf{a} is denoted by \mathbf{a}^T . The Euclidean norm of a vector and degenerate interval are denoted by $\|\cdot\|$ and $[a, b] = \{x | a \leq x \leq b\}$, respectively.

II. SYSTEM MODEL

A. UAV-BSs and Users

We consider a HAP and multiple UAVs as aerial BSs, which are denoted by $\mathcal{U} = \{1, \dots, U\}$, where U is the total number of UAV-BSs. We assume that we have M users in our environment, $\mathcal{M} = \{1, \dots, M\}$ and each UAV-BS can serve at most L users, and we denote L_u to be the maximum number of users allocated to UAV-BS u . Time is considered to be slotted and normalized to the slot duration (i.e., the slot duration is taken as 1), and the UAV-BSs' operating period is T time slots, where $\mathcal{T} = \{0, 1, \dots, T\}$. The coordinates of the m -th user can be expressed as $\mathbf{v}_m(t) = [x_m(t), y_m(t)]^T$, where $x_m(t)$ and $y_m(t)$ are the X-coordinate and Y-coordinate of user m in time slot t , respectively. The location of the HAP is denoted by $\mathbf{q}_{\text{HAP}} = [x_{\text{HAP}}, y_{\text{HAP}}, h_{\text{HAP}}]^T$, which is considered constant during the operation time of the network, and the location of UAV-BS u is denoted by $\mathbf{q}_u(t) = [x_u(t), y_u(t), h_u(t)]^T$, in which $h_u(t) \in [h_{\min}, h_{\max}]$. Furthermore, the trajectories of UAV-BSs are also subject to the collision avoidance constraint, i.e.,

$$C1 : \|\mathbf{q}_u(t) - \mathbf{q}_{u'}(t)\| \geq d_{\min}, \forall u \neq u', \forall t \in \mathcal{T}, \quad (1)$$

where d_{\min} denotes the minimum inter UAV-BS distance. Let $v_u(t)$ be the velocity of UAV-BS u at time slot t . As a result of the mechanical limitation, the maximum speed of each UAV-BS is v_{\max} . We assume that the initial location of UAV-BSs is random and users are already assigned to UAV-BSs based on the quality of their channels; and by that, we have a distance-based coverage area for each UAV-BS to serve its users. As a result, we have the following constraints:

$$C2 : \begin{cases} \min_{m \in \mathcal{M}} x_m(t) \leq x_u(t) \leq \max_{m \in \mathcal{M}} x_m(t), \\ \min_{m \in \mathcal{M}} y_m(t) \leq y_u(t) \leq \max_{m \in \mathcal{M}} y_m(t). \end{cases} \quad (2)$$

In the users' side, we assume that if they have any update at time slot t , they transmit their task to the assigned UAV-BSs via wireless link. We assume that each user has a set of

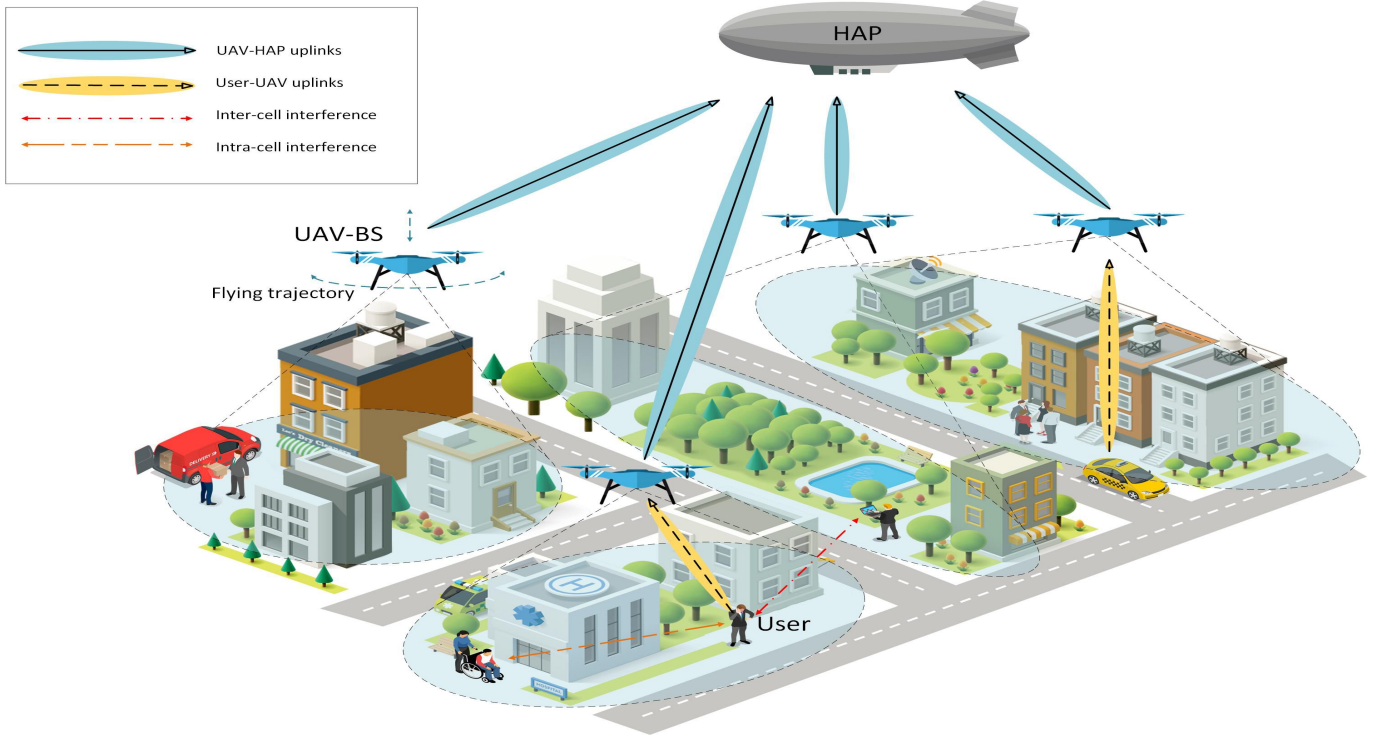


Fig. 1: System model: Hierarchical NTN, user-UAV and UAV-HAP links.

tasks \mathcal{S} to be sent and processed, in which $\mathcal{S} = \{1, \dots, S\}$, where S is the maximum number of tasks. Let $I_{m,s}(t)$ be the indicator of whether user m has task s to send $I_{m,s}(t) = 1$ or not $I_{m,s}(t) = 0$.

B. Channel Model

We consider a multi-carrier NOMA system model for transmitting data from users to UAV-BSs. If users have data, they will transmit their data updates to the UAV-BS, independently from other users, through N subcarriers (SCs) at time slot t . We denote the indices of subcarriers by $\mathcal{N} = \{1, 2, \dots, N\}$, where N is the total number of subchannels. Let $K_m^{u,n}(t)$ be the indicator whether UAV-BS u allocates SC n to user m at time slot t , ($K_m^{u,n}(t) = 1$) or not ($K_m^{u,n}(t) = 0$). Note that at each time slot, a user can only transmit its task through one subchannel to one UAV-BS at time slot t , i.e. $\sum_{n \in \mathcal{N}} K_m^{u,n}(t) \leq 1$. Furthermore, each subchannel is allocated to a maximum of two users at time slot t , i.e. $\sum_{m \in \mathcal{M}} K_m^{u,n}(t) \leq 2$. The UAV-BS receives the superimposed message signal of different users and applies SIC to decode each signal. The channel gain from user m assigned to UAV-BS u on SC n is denoted by

$$g_m^{u,n}(t) = \frac{\beta_0}{d_m^u(t)^2}, \quad (3)$$

$$d_m^u(t) = \sqrt{(x_u(t) - x_m^u(t))^2 + (y_u(t) - y_m^u(t))^2 + h_u(t)^2},$$

where β_0 denotes the power gain of a channel with reference distance $d_0 = 1$ m and $d_m^u(t)$ denotes the distance between the UAV-BS u and user m at time slot t . The channel gains of all users belonging to UAV-BS u on SC n are sorted as

$|g_1^{u,n}|^2 \leq \dots \leq |g_m^{u,n}|^2 \leq \dots \leq |g_M^{u,n}|^2$. We assume that all users are decoded by SIC based on these levels of channel conditions, i.e., the data signals of users in the strong channel conditions must be decoded after the data signals of users in the weak channel conditions are subtracted. We define a permutation $\zeta : \mathcal{M} \rightarrow \mathcal{M}$ to denote the SIC decoding order. For example, if the UAV-BS decodes the users' signals with the order $3 \rightarrow 1 \rightarrow 2$, the permutation ζ is set to $\zeta(1) = 3$, $\zeta(2) = 1$, $\zeta(3) = 2$. According to [32], the data rate transmitted from the user m on SC n received at the UAV-BS u at time slot t , can be expressed as

$$R_m^{u,n}(t) = B_n \log_2 \left(1 + \frac{G_{\zeta(m)}^{u,n}(t) p_{\zeta(m)}^{u,n}(t) K_{\zeta(m)}^{u,n}(t)}{I_{\zeta(m), \text{intra}}^{u,n}(t) + I_{\zeta(m), \text{inter}}^{u,n}(t) + 1} \right), \quad (4)$$

where the first term in denominator represents interference between users of SC n of u -th UAV-BS and the second term denotes to interference from other UAV-BSs' users to users in SC n of UAV-BS u , and we have

$$I_{\zeta(m), \text{intra}}^{u,n}(t) = \sum_{i=m+1}^M K_{\zeta(i)}^{u,n}(t) G_{\zeta(i)}^{u,n}(t) p_{\zeta(i)}^{u,n}(t), \quad (5)$$

$$I_{\zeta(m), \text{inter}}^{u,n}(t) = \sum_{\substack{u' \in \mathcal{U} \\ u' \neq u}} \sum_{j=m+1}^M K_{\zeta(j)}^{u',n}(t) G_{\zeta(j)}^{u',n}(t) p_{\zeta(j)}^{u',n}(t),$$

where $B_n = \frac{B}{N}$, $p_m^{u,n}(t)$ and $G_m^{u,n}(t)$ represent the bandwidth of SC n , assigned power for the user m of UAV-BS u on SC n at time slot t , and normalized channel gain to power of additive noise $G_m^{u,n}(t) = |g_m^{u,n}(t)|^2 / \sigma_z^2$, respectively. B is the

bandwidth of each UAV-BS. Also, power of each user should satisfy

$$C3: \sum_{n \in \mathcal{N}} K_m^{u,n}(t) p_m^{u,n}(t) \leq p^{\max}, \forall u \in \mathcal{U}, \forall m \in \mathcal{M}, \quad (6)$$

where p^{\max} is the maximum power constraint for each user. It is assumed that the UAV-BS that receives the user's task will process only as much as it has been allocated computing capacity for, and will send the remainder to the HAP; and since this is not possible within the same time slot as the task is received, it is stored in a memory in order to be sent in the next time slots. Hence, the binary variable for sending the task of user m that remained in UAV-BS u to the HAP at time slot t is set to $\phi_{m,s}^{u,\text{HAP}}(t) = 1$ in this case, and $\phi_{m,s}^{u,\text{HAP}}(t) = 0$, otherwise. The transmission rate of the UAV-BS u to the HAP at time slot t is formulated as follows:

$$R^{u,\text{HAP}}(t) = B^{u,\text{HAP}} \log_2 \left(1 + \frac{p^{u,\text{HAP}}(t) G^{u,\text{HAP}} L_s L_l \phi_{m,s}^{u,\text{HAP}}(t)}{k_B T_{\text{temp}} B^{u,\text{HAP}}} \right), \quad (7)$$

$$\forall u \in \mathcal{U}, m \in \mathcal{M}, t \in \mathcal{T},$$

where $B^{u,\text{HAP}}$ and $G^{u,\text{HAP}}$ are bandwidth of UAV-HAP channel and antenna power gain, respectively. Also, L_l is the total line loss, and $L_s = \left(\frac{c}{4\pi d^{u,\text{HAP}}(t) f^{u,\text{HAP}}} \right)^2$ is the free space path loss. Furthermore, k_B , $f^{u,\text{HAP}}$, and T_{temp} denote the Boltzmann's constant, center frequency, and the system noise temperature, respectively. Wherein, c is the speed of light, $d^{u,\text{HAP}}(t)$ is the distance between UAV-BS u and the HAP calculated by (8) below, and $f^{u,\text{HAP}}$ is the center frequency:

$$d^{u,\text{HAP}}(t) = \sqrt{(x_u(t) - x_{\text{HAP}})^2 + (y_u(t) - y_{\text{HAP}})^2 + (h_u(t) - h_{\text{HAP}})^2}, \quad (8)$$

$$\forall u \in \mathcal{U}, t \in \mathcal{T}.$$

$p^{u,\text{HAP}}(t)$ is the transmit power of UAV-BS u . Transmit power of each UAV-BS should satisfy

$$C4: \phi_{m,s}^{u,\text{HAP}}(t) p^{u,\text{HAP}}(t) \leq p^{u,\max}, \quad (9)$$

$$\forall u \in \mathcal{U}, m \in \mathcal{M}, s \in \mathcal{S}, t \in \mathcal{T},$$

where $p^{u,\max}$ is the maximum transmit power of each UAV-BS.

C. Computing Capacity Allocation

If UAV-BS u has sufficient computing capacity, the transmitted part of task s of user m will be executed. Therefore, we assign a variable $\theta_{m,s}^u(t) \in [0, 1]$ to capture the amount of allocated computing capacity to task s of user m at UAV-Bs u at time slot t . We denote $C_{m,s}^u(t)$ to be the computing capacity of the UAV-BS u allocated to compute the task s of user m at time slot t that can be calculated as follows:

$$C_{m,s}^u(t) = \theta_{m,s}^u(t) c^u \alpha_{m,s}(t), \forall u \in \mathcal{U}, m \in \mathcal{M}, s \in \mathcal{S}, t \in \mathcal{T}, \quad (10)$$

where $\alpha_{m,s}(t)$ and c^u are the fraction of tasks sent from the task s of the user m , which is equal to data rate of that user in time slot t , and the computing capacity of one bit of data.

Our assumption is that the size of computation tasks is fixed and the same for all users and it is denoted by $\alpha_{m,s}$. Taking into account the maximum capacity available in each UAV-BS, C_u^{\max} , the following requirement must hold

$$C5: C_{\text{usage}}^u(t) = \sum_{m \in \mathcal{M}} \sum_{s \in \mathcal{S}} C_{m,s}^u(t), C_{\text{usage}}^u(t) \leq C_u^{\max}, \quad (11)$$

$$\forall u \in \mathcal{U}, t \in \mathcal{T}.$$

On the HAP side, we consider $\eta_{m,s}(t) \in [0, 1]$ to be the amount of allocated computing capacity to task s of user m . By considering $C_{m,s}^{\text{HAP}}(t)$ to be the allocated computing capacity of the HAP to task s of user m at time slot t , we have

$$C_{m,s}^{\text{HAP}}(t) = \eta_{m,s}(t) c^{\text{HAP}} \beta_{m,s}^u(t), \forall u \in \mathcal{U}, m \in \mathcal{M}, s \in \mathcal{S}, t \in \mathcal{T}, \quad (12)$$

where $\beta_{m,s}^u(t)$ is the amount of task s of user m sent from UAV-BS u to the HAP, which is equivalent to the amount of data rate at time slot t , and c^{HAP} represents the computing capacity of one bit of data in the HAP. Taking into account the maximum capacity available in HAP, C_{HAP}^{\max} , the following requirement must be satisfied

$$C6: C_{\text{usage}}^{\text{HAP}}(t) = \sum_{m \in \mathcal{M}} \sum_{s \in \mathcal{S}} C_{m,s}^{\text{HAP}}(t), C_{\text{usage}}^{\text{HAP}}(t) \leq C_{\text{HAP}}^{\max}, \forall t \in \mathcal{T}. \quad (13)$$

D. Remaining Tasks of the User, the UAV-BS and the HAP

1) *User Side*: Assuming that all tasks can take more than one time slot to be transmitted, we calculate the remaining task of each user in user side at each time slot $\alpha_{m,s}^{\text{rem}}(t)$, and it can be represented as

$$\alpha_{m,s}^{\text{rem}}(t) = \alpha_{m,s}^{\text{rem}}(t-1) - \alpha_{m,s}(t), \alpha_{m,s}^{\text{rem}}(0) = \alpha_{m,s}, \quad (14)$$

$$\forall m \in \mathcal{M}, s \in \mathcal{S}, t \in \mathcal{T}.$$

2) *UAV-BS Side*: The remaining tasks in UAV-BS u at time slot t can be expressed as

$$O_{m,s}^u(t) = (1 - \theta_{m,s}^u(t)) K_m^u(t) I_{m,s}(t) \alpha_{m,s}(t) \quad (15)$$

$$+ \sum_{\tau=1}^{t-1} (1 - \phi_{m,s}^{u,\text{HAP}}(t-\tau)) (1 - \theta_{m,s}^u(t-\tau))$$

$$K_m^u(t-\tau) I_{m,s}(t-\tau) \alpha_{m,s}(t-\tau)$$

$$- \phi_{m,s}^{u,\text{HAP}}(t) \beta_{m,s}^u(t), \forall u \in \mathcal{U}, m \in \mathcal{M}, s \in \mathcal{S}, t \in \mathcal{T},$$

where $K_m^u(t)$ denotes to whether UAV-BS u allocates a subchannel to user m ($K_m^u(t) = 1$) or not ($K_m^u(t) = 0$), and $O_{m,s}^u(t)$ represents the fraction of task s of user m located in UAV-BS u . It should be mentioned that different parts of a task from one user may be sent to different UAV-BSSs. In (15), the first term indicates the amount of tasks that are sent to the UAV-BS in time slot t , but the computing capacity is not sufficient to process them. The second term indicates the

amount of tasks that were sent in the previous time slots to UAV-BS and, in addition to not being processed, they were not sent to the HAP either. Finally, the third term is the amount of tasks that are sent to the HAP at time slot t . Therefore, to calculate the remaining tasks of users in UAV-BS u , we have

$$O^u(t) = \sum_{m \in \mathcal{M}} \sum_{s \in \mathcal{S}} O_{m,s}^u(t), \forall u \in \mathcal{U}, t \in \mathcal{T}. \quad (16)$$

3) *HAP Side*: The remaining tasks of users in the HAP at time slot t can be calculated as

$$O^{\text{HAP}}(t) = \sum_{\tau=0}^{t-1} \sum_{u \in \mathcal{U}} \sum_{m \in \mathcal{M}} \sum_{s \in \mathcal{S}} (1 - \eta_{m,s}(t - \tau)) \phi_{m,s}^{u,\text{HAP}}(t - \tau) \beta_{m,s}^u(t - \tau), \quad (17)$$

in which it indicates the tasks that are entered into the HAP at time slot t and earlier times, but there is not enough capacity to process them.

In Fig. 2, an example of system operation for task s of user m is demonstrated, in which the X-axis refers to the time slot and the Y-axis refers to the user/UAV-BS transmission and CPU allocation in UAV-BSs and the HAP. A portion of the task is received in the UAV-BS during the first time slot (in dark yellow), but there is no computing capacity available. It must be sent to the HAP in the next time slot. During the second time slot, another part of the task is sent to the UAV-BS, which may be different from the previous UAV-BS. Computing capacity is sufficient for this part of the task (in red). The remaining task from the previous time slot is forwarded to the HAP (in light green) and capacity is allocated (in dark green). In the third time slot, no channel is assigned to the user. During the fourth time slot, however, the channel is assigned to the user, and computing capacity is allocated to a portion of the transmitted task, with the remainder sent to the HAP. The next task s' of the user can be generated in the fifth time slot, while the remaining task from the UAV-BS is forwarded to the HAP to be processed. In the end, the whole task is processed, partially in UAV-BSs (in red) and partially in the HAP (in dark green).

E. Age of Information

Due to the importance of freshness of data at receiver side, we use the AoI matrix to measure information timeliness. Let $F_{m,s}$ be the time at which the most up-to-date task s was generated in user m

$$A_m(t) = \begin{cases} t - F_{m,s}, & \text{if (18b),} \\ A_m(t-1) + 1, & \text{otherwise,} \end{cases} \quad (18a)$$

$$\sum_{\tau=0}^t \sum_{u \in \mathcal{U}} C_{m,s}^u(\tau) + \sum_{\tau=0}^t C_{m,s}^{\text{HAP}}(\tau) \geq \alpha_{m,s}, \forall m \in \mathcal{M}, s \in \mathcal{S}, \quad (18b)$$

where $A_m(t)$ is the AoI of user m at time slot t , which we interpret it as follows: as long as a task has not been fully received and processed, the AoI of user increases by one for each time slot, and the value of the AoI of a user equals to the time elapsed since receiving the last task of that user.

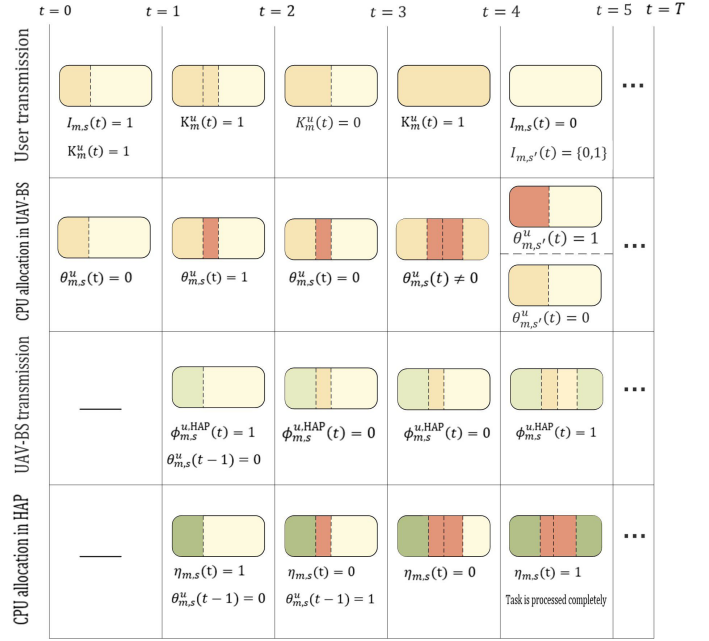


Fig. 2: An example of the system operation.

We are able to calculate the AoI of the user based on (18b), which indicates that all the allocated computing capacity on both UAV-BS and HAP sides must be greater than or equal to the task size. To be more specific, there are three cases of increasing the AoI for each user. In the first case, the user has a task to send but UAV-BS does not allocate any subchannel for the task; in the second case, the user has a task and a channel for sending it, but the total allocated computing capacity is less than the user's task; and in the third case, the user sends the part or all of a task to HAP through UAV-BS but the total allocated computing capacity in both sides of UAV-BSs and HAP is less than the user's task.

F. Stochastic Channel Uncertainty

Owing to the inherent random nature of wireless channels, it is impossible to obtain perfect CSI. As such, channel uncertainties are considered in this subsection. Assuming the channel estimation error follows the Gaussian CSI error model [33]–[35], we have

$$\mathcal{R}_g = \{G_m^{u,n} | \hat{G}_m^{u,n} + \Delta G_m^{u,n}, \Delta G_m^{u,n} \sim \mathcal{CN}(0, \sigma_e^2)\}, \quad (19)$$

where $\hat{G}_m^{u,n}$ denotes channel estimation value that are known at the transmitters by channel estimation algorithms and channel feedback [36] and $\Delta G_m^{u,n}$ corresponds to estimation error with the variances σ_e^2 . To ensure minimum SINR requirement of each user, we put a constraint on data rate:

$$R_m^{u,n}(t) \geq R_{\min}, \forall u \in \mathcal{U}, m \in \mathcal{M}, \quad (20)$$

$$n \in \mathcal{N}, t = \{t | K_m^u(t) = 1, t \in \mathcal{T}\},$$

where R_{\min} is minimum rate requirement of all users. We can limit the actual outage rate probability of each user within a

threshold value and achieve a trade-off between optimality and robustness

$$C7: \Pr[R_m^{u,n}(t) \leq R_{\min} | \Delta G_m^{u,n} \in \mathcal{R}_g] \leq \epsilon_m, \quad (21)$$

$$\forall u \in \mathcal{U}, m \in \mathcal{M}, n \in \mathcal{N}, t = \{t | K_m^u(t) = 1, t \in \mathcal{T}\}.$$

G. Problem Formulation

The objective of this paper is to minimize the AoI of all users subject to UAV-BS trajectory and power and computing capacity allocation in NTN under CSI uncertainty constraint. Our problem for $t \in \mathcal{T}$ can be formulated as follows:

$$\min_{\mathbf{v}_{\mathcal{U}}, \mathbf{K}, \mathbf{P}_{\mathcal{M}}, \boldsymbol{\theta}, \mathbf{P}_{\mathcal{U}}, \boldsymbol{\eta}} \left\{ A_{\mathcal{M}}^{\mathcal{T}} = \sum_{t=0}^T \sum_{m=0}^M A_m(t) \right\} \quad (22a)$$

$$\text{s.t. } C1 - C7, \quad (22b)$$

$$\sum_{n \in \mathcal{N}} K_m^{u,n}(t) \leq 1, \forall u \in \mathcal{U}, \forall m \in \mathcal{M}, t \in \mathcal{T}, \quad (22c)$$

$$\sum_{m \in \mathcal{M}} K_m^{u,n}(t) \leq 2, \forall u \in \mathcal{U}, \forall n \in \mathcal{N}, t \in \mathcal{T}, \quad (22d)$$

$$h_{\min} \leq h_u(t) \leq h_{\max}, \forall u \in \mathcal{U}, t \in \mathcal{T}, \quad (22e)$$

$$v_u(t) \leq v_{\max}, \forall u \in \mathcal{U}, t \in \mathcal{T}, \quad (22f)$$

where $\mathbf{v}_{\mathcal{U}} = \{v_u(t), u \in \mathcal{U}\}$, $\mathbf{K} = \{K_m^{u,n}(t), u \in \mathcal{U}, m \in \mathcal{M}, n \in \mathcal{N}\}$ and $\mathbf{P}_{\mathcal{M}} = \{p_m^{u,n}(t), u \in \mathcal{U}, m \in \mathcal{M}, n \in \mathcal{N}\}$ denote the velocity of all UAV-BSs, channel allocation between users and UAV-BS and transmission power allocation of all users, respectively. $\boldsymbol{\theta} = \{\theta_{m,s}^u(t), u \in \mathcal{U}, m \in \mathcal{M}, s \in \mathcal{S}\}$ denotes the CPU allocation to tasks of users in all UAV-BSs. Moreover, $\mathbf{P}_{\mathcal{U}} = \{p^{u,\text{HAP}}(t), u \in \mathcal{U}\}$ and $\boldsymbol{\eta} = \{\eta_{m,s}(t), m \in \mathcal{M}, s \in \mathcal{S}\}$, denote the transmission power of all UAV-BSs and computing capacity allocation in the HAP, respectively.

III. MADDPG AND FRL APPROACHES TO SOLVE THE PROBLEM

The optimization problem (22) is a mixed integer non-linear programming (MINLP) problem, which is non-convex and difficult to solve globally. In this section, we adopt online learning based algorithms to handle the resource allocation and trajectory planning. To do so, we have to reformulate it as Markov Decision Process (MDP) and then apply two DRL-based algorithms to solve it.

A. Markov Decision Process

In this problem we deal with two kinds of agents, a HAP and multiple UAV-BSs, as they choose their own actions. However, both types of agents follow the same goals, which are minimizing average AoI. Agents gradually learn the model-free policy that maps observations into optimal actions. In the DRL framework, MDP is a tuple $\{s_t, a_t, r_t, s_{t+1}\}$ containing states, actions, rewards, and new states:

States $s_{s,t} = \{s_{s,t}^u, s_{s,t}^{\text{HAP}}\}$, $s_{s,t} \in \mathcal{S}_s, u \in \mathcal{U}$: At each time slot t , the set of states of UAV-BS u is expressed as

$$s_{s,t}^u = \{\mathbf{q}_u(t), \mathbf{v}_m(t), I_{m,s}(t), C_{\text{usage}}^u(t), \alpha_{m,s}^{\text{rem}}(t), O^u(t), A_m(t)\}. \quad (23)$$

The states of UAV-BS u include location of UAV-BS and users, binary variable of existing task in network, amount of CPU usage, remaining tasks on both user and UAV-BS sides, and also the AoI values of all users. At each time slot t , the set of states of HAP is defined as

$$s_{s,t}^{\text{HAP}} = \{\mathbf{q}_{\mathcal{U}}(t), I_{m,s}(t), C_{\text{usage}}^{\text{HAP}}(t), O^{\text{HAP}}(t), O^{\mathcal{U}}(t-1), A_m(t)\}. \quad (24)$$

The states of HAP include location of all UAV-BSs, binary variable of existing task in network, amount of CPU usage in HAP, remaining tasks in HAP side, and remaining tasks of previous time slots of all UAV-BSs, and also the AoI values of all users.

Actions $a_t = \{a_t^U, a_t^{\text{HAP}}\}$, $a_t \in \mathcal{A}, u \in \mathcal{U}$: At each time slot t , the actions that are taken by each of UAV-BS and HAP are

$$a_t^u = \{v_u(t), K_m^{u,n}(t), p_m^{u,n}(t), \theta_{m,s}^u(t)\}, \quad (25)$$

$$a_t^{\text{HAP}} = \{p^{u,\text{HAP}}(t), \eta_{m,s}(t)\}. \quad (26)$$

The actions of each UAV-BS in each time slot comprise taking velocity in each direction which results in trajectory decision, subchannel allocation and power allocation to users, and CPU allocation to task of all users. The actions of the HAP comprise power allocation to UAV-BSs and CPU allocation to task of all users. Since we clip the action values in $[-1, 1]$, for integer actions we denote 1 for action value in $[0, 1]$ and 0 for action value in $[-1, 0]$.

Reward r_t : To minimize the average AoI of all users, we define the reward as

$$r_t = -\left\{ \frac{1}{M} \sum_m A_m(t) \right\}, \forall m \in \mathcal{M}. \quad (27)$$

Discount Factor γ : The long-term accumulated reward of a policy is modeled as

$$R_t = \sum_{i=0}^{\infty} \gamma^i r_{t+i}, \quad (28)$$

where the discount factor $\gamma \in [0, 1]$ indicates that the agent is more concerned about the long-term reward if the discount factor approaches 1. In addition, the transition function $T(s_{s,t}, a_t, s_{s,t+1})$ identifies the probability of the next state $s_{s,t+1} \in \mathcal{S}_s$ given the current state $s_{s,t} \in \mathcal{S}_s$ and the current action $a_t \in \mathcal{A}$ that applies on $s_{s,t}$.

B. MADDPG Approach

This approach utilizes actor-critic networks, in which each agent is equipped with four networks: actor, target actor, critic, and target critic network. The observations and actions of all RL agents are considered for learning the actor and critic networks [37]. During action execution, each agent's actor network only considers local observations, but observations of all agents along with each agent's actions are fed into critic networks of that agent to be evaluated. Based on a consistent gradient signal, each agent learns an optimal policy through centralized training and decentralized execution. To improve the online learning efficiency, the replay buffer technique is used. However, the batch size is chosen to be as small as possible. Considering a policy π , each observation maps to

an action. The value function, based on which the quality of policy is evaluated, is defined as

$$Q_\pi = \mathbb{E} \left[\sum_{t=0}^T \gamma^t r(s_t, a_t) \right]. \quad (29)$$

Through optimization of the objective function, π is parameterized to π_θ , and its expected value is maximized $J(\theta) = \mathbb{E}[Q_{\pi_\theta}(s, \pi_\theta(s))]$. The gradient of this objective function can be calculated by applying the deterministic policy gradient and the chain rule is applied to the expected reward from the distribution J to update the policy function π .

$$\begin{aligned} \nabla_{\theta\pi} J &\approx \mathbb{E}_{s_t \sim \rho^\beta} \left[\nabla_{\theta\pi} Q(s, a | \theta^Q) \Big|_{s=s_t, a=\pi(s_t|\theta^\pi)} \right], \\ &= \mathbb{E}_{s_t \sim \rho^\beta} \left[\nabla_a Q(s, a | \theta^Q) \Big|_{s=s_t, a=\pi(s_t)} \nabla_{\theta\pi} \pi(s | \theta^\pi) \Big|_{s=s_t} \right], \end{aligned} \quad (30)$$

where ρ^β is the distribution of state-visitation associated with a policy. By copying directly (hard update) or exponentially decaying average (soft update), defined by hyper parameter $\tau \ll 1$, the target network is synchronized with the primary network every T_{up} steps. In Algorithm 1, the process of learning in this approach is presented, with considering FRL-mode to be False.

C. VFRL Approach

In the proposed model, we are dealing with two types of agents and although they are in the same environment, they have different interactions with environment. This leads us to apply the vertical category of FRL algorithm (VFRL) to our problem [38]. Due to the decentralized nature of the model, a peer-to-peer (P2P) method has been suggested [39], in which there is no central aggregator to form a global model for all agents and they exchange their parameters among themselves. As a result, we assume that at every T_{FL} steps, each agent trains the model on its local data, resulting in a model with parameter θ for the actor network. Then, each agent aggregates and averages updates from all other agents. Next, the local model parameters are updated by

$$\theta_t^i = \omega^i \theta_t^i + \sum_{i'} \omega^{i'} \theta_t^{i'}, \quad (31)$$

where i refers to index of agents and ω^i is the weight of parameters of agent i . According to [29], we consider the weights as $\omega^i = \frac{1}{N_{agent}}$ and $\omega^{i'} = \frac{1-\omega^i}{N_{agent}-1}$, where N_{agent} is the number of agents. Inspired by [40], [41], we develop Algorithm 1, which is in VFRL mode, when FRL-mode is True and MADDPG, otherwise.

D. Computational Complexity

We analyze the computational complexity of both MADDPG and P2P-VFRL approaches. The complexity of DNN-based algorithms depends on the architecture, configuration, number of inputs and outputs, and hidden layers. Moreover, we have to take into account the action and state space size, number of neural networks, number of trainable variables, and the communication overhead between agents and the central

Algorithm 1: Online P2P-VFRL and MADDPG. The agents are indexed by i ; B and D are batch size and local mini-batch size, respectively, and α , β are the learning rates of actor and critic networks.

Input: Initialize parameters ϕ and θ of critic and actor networks Q and μ , target networks Q' and μ' ; set $M = 0$ as memory counter

- 1 Receive initial states
- 2 **for** episode $t = 1$ **to** T **do**
- 3 **for** each agent $i \in \{1, \dots, U, H\}$ **do**
- 4 Observe $s_{s,t,i}$ and select action $a_{t,i} = \mu_{\theta_i}(s_{s,t,i})$
- 5 Execute actions and observe reward $r_{t,i}$ and new states $s_{s,t+1,i}$
- 6 Store $(s_{s,t}, a_t, r_t, s_{s,t+1})$ in replay buffer \mathcal{D} and $\mathbf{s}_{s,t} \leftarrow \mathbf{s}_{s,t+1}$
- 7 $M \leftarrow M+1$
- 8 **if** $M \geq B$ **then**
- 9 Sample mini-batch of size D , $(\mathbf{s}_{s,t}^j, \mathbf{a}_t^j, \mathbf{r}_t^j, \mathbf{s}_{s,t+1}^j)$ from replay buffer \mathcal{D}
- 10 **for** each agent i **do**
- 11 Set
- 12 $y^j = r^j + \gamma Q'(\mathbf{s}_{s,t+1}^j, \mathbf{a}_{t+1}^j | \theta')$ $\Big|_{\mathbf{a}_{t+1}^j = \mu'(\mathbf{s}_{s,t+1}^j)}$
- 13 Calculate:
- 14 $\mathcal{L} = \frac{1}{D} \sum_j (y^j - Q(\mathbf{s}_s^j, \mathbf{a}^j | \phi))^2$
- 15 **if** $t \bmod T_{FL} == 1$ **and** FRL-mode **then**
- 16 **for** each agent i **in parallel do**
- 17 $\theta_{t+1}^i \leftarrow \text{AgentUpdate}(i, \theta, \phi, \alpha, \beta)$
- 18 $\theta_{t+1}^i = \omega^i \theta_{t+1}^i + \sum_{i'} \omega^{i'} \theta_{t+1}^{i'}$
- 19 **else**
- 20 **for** each agent i **in parallel do**
- 21 $\theta_{t+1}^i \leftarrow \text{AgentUpdate}(i, \theta, \phi, \alpha, \beta)$
- 22 **if** $t \bmod T_{up} == 1$ **then**
- 23 Update target networks parameters for each agent i :
- 24 $\theta_t^i \leftarrow \tau \theta_t^i + (1 - \tau) \theta_t^i$
- 25 $\phi_t^i \leftarrow \tau \phi_t^i + (1 - \tau) \phi_t^i$
- 26 **Function** $\text{AgentUpdate}(i, \theta, \phi, \alpha, \beta)$:
- 27 Update actor using the sampled policy gradient:
- 28 $\nabla_{\theta} J \approx \frac{1}{D} \sum_j \left\{ \nabla_{\theta} \mu(\mathbf{s}_s^j) \nabla_a Q(\mathbf{s}_s, \mathbf{a} | \phi) \Big|_{\mathbf{s}_s = \mathbf{s}_s^j, \mathbf{a} = \mu(\mathbf{s}_s^j)} \right\}$
- 29 Update critic by minimizing the loss: \mathcal{L}
- 30 $\theta_{t+1}^i = \theta_t^i - \alpha \nabla \mathcal{L}(\theta_t^i)$
- 31 $\phi_{t+1}^i = \phi_t^i - \beta \nabla \mathcal{L}(\phi_t^i)$
- 31 **return** $\theta_{t+1}^i, \phi_{t+1}^i$

servers. To this end, we assume $|S_s|$ and $|A|$ to be action and state space size, respectively; which according to (23), (24) and (25), are calculated as follows:

$$\begin{aligned} |S_s| &= \underbrace{2 \times M + 4 \times (M \times S) + 3 \times U + M}_{\text{UAV-BS states}=|S_s^u|} \\ &\quad + \underbrace{3 \times U + 3 \times (M \times S) + M + (U \times M \times S)}_{\text{HAP states}=|S_s^{\text{HAP}}|}, \\ |A| &= \underbrace{3 + 2 \times (M \times N) + (M \times S)}_{\text{UAV-BS actions}=|A^u|} \\ &\quad + \underbrace{(M \times U) + (M \times S)}_{\text{HAP actions}=|A^{\text{HAP}}|}. \end{aligned} \quad (32)$$

Thus, the number of MADDPG parameters to train is

$$\mathcal{O}(U^2(|S_s^u| + |A^u|) + H^2(|S_s^{\text{HAP}}| + |A^{\text{HAP}}|)), \quad (34)$$

where U and H represent the number of UAV-BSs and HAP agents, respectively. MADDPG employs $2 \times (N_{agents}(\frac{1}{2}Q + \frac{1}{2}A))$ neural networks as was with P2P-VFRL, where the multiplication by 2 is due to target networks, and $\frac{1}{2}Q$ and $\frac{1}{2}A$ represent the critic and actor networks. Moreover, $N_{agents} = U + H$ refers

to number of agents. To calculate the computational complexity, first we assume that Γ_i^a , and Γ_i^c are the number of neurons in the i -th layer of the actor and critic networks, respectively. We denote L_a and L_c to be the total number of layers in the respective actor, and critic networks. As actor and critic networks are fully interconnected, their computational complexity can be expressed as $\mathcal{O}(\sum_{i=2}^{L_a-1}(\Gamma_{i-1}^a\Gamma_i^a + \Gamma_i^a\Gamma_{i+1}^a))$, and $\mathcal{O}(\sum_{i=2}^{L_c-1}(\Gamma_{i-1}^c\Gamma_i^c + \Gamma_i^c\Gamma_{i+1}^c))$, respectively. As a result, the computational complexity of both approaches can be obtained as

$$\mathcal{O}(N_{\text{agents}} \cdot D \cdot E_{\text{episode}} \cdot (\mathfrak{C}^a + \mathfrak{C}^c)), \quad (35)$$

where D and E_{episode} indicate the mini-batch sampling size, and number of episodes, respectively. In addition we have $\mathfrak{C}^a = \sum_{i=2}^{L_a-1}(\Gamma_{i-1}^a\Gamma_i^a + \Gamma_i^a\Gamma_{i+1}^a)$ and $\mathfrak{C}^c = \sum_{i=2}^{L_c-1}(\Gamma_{i-1}^c\Gamma_i^c + \Gamma_i^c\Gamma_{i+1}^c)$. Most multi-agent reinforcement learning-based frameworks rely on agents' communication. For the learning process to be stabilized and agents to cooperate, data exchange is essential which imposes some overhead on the system. To obtain the communication overhead in the proposed framework, we examined how often the agents need to interact with the central server and other agents during the learning process. Accordingly, P2P-VFRL has an overhead of N_{agents} , while MADDPG has an overhead of $N_{\text{agents}}(N_{\text{agents}} - 1)$.

IV. NUMERICAL RESULTS

A. Simulation setup

We consider one HAP with the height of 20 km, and for the initial step, 2 UAV-BSs with an altitude of 400 m are uniformly distributed in the area with size of 200 km \times 200 km, and terrestrial mobile users are randomly distributed in this area. The task size of all users $\alpha_{m,s}$ is fixed to 10 Mbit. At the beginning of the simulation, we assume that all users are assigned tasks to send. After completing each task, the next task of the user will be generated randomly with the probability of 50%. Furthermore, we assume that the total bandwidth of each UAV is $B = 10$ MHz, which is divided into $N = 8$ subchannels. The AWGN power spectrum density is -174 dBm/Hz. Each subchannel can be assigned to at most 4 users and each user can access 2 subchannels. The parameters associated with computation and communication are summarized in Table II. Furthermore, since users have to send high volume tasks, the maximum number of users is assumed to be 40. Also, to deploy DNN, we use Pytorch library in Python.

B. Simulation Results Discussions

A comparison of the rewards of the two approaches with different levels of uncertainty (including perfect CSI) is provided in Fig. 3, in which users send five tasks to be processed and agents allocate resources until all tasks are processed. It is observed that the MADDPG approach has better performance, as it is shown in Table III. The reason is that it relies on central training and decentralized execution. After central training in MADDPG, agents may finally have different models for actor

TABLE II: Simulation Parameters

Parameter	Value
c^u	200 cycles/bit
c^{HAP}	500 cycles/bit
$p^{u,\max}$	0.5 W
p^{\max}	0.2 W
k_B	1.38×10^{-23} J/K
T_{temp}	1000 K
$G^{u,\text{HAP}}$	15 dB
$B^{u,\text{HAP}}$	20 MHz
$f^{u,\text{HAP}}$	2.4 GHz
v_{\max}	50 m/s
C_u^{\max}	10^9 cycles
C_{HAP}^{\max}	5×10^9 cycles
Fast fading	Rayleigh fading
Neural network parameter	
Replay buffer size	50000
Mini batch size	8
Number/size of actor networks hidden layers	2/1024, 512
Number/size of critic networks hidden layers	2/512, 256
Critic/Actor networks learning rate	0.0001/0.00001
Discount factor	0.99
Target networks soft update parameter, τ	0.0005

networks. On the other hand, in P2P-VFRL we deal with aggregating other agents' network parameters and updating their parameters at specific time slots and decentralized training is applied in the training phase, with decentralized execution. Given the better results achieved by MADDPG, we evaluate the effects of the main parameters with this approach including maximum available computation capacity both in UAV-BS and HAP, maximum transmission power of each user and UAV-BS, number of subchannels with considering the number of users, and uncertainty, and also the effect of task size. The source code for the simulation of both approaches are available in [42].

1) *Maximum Available CPU*: To evaluate the impact of existing computation capacity in UAV-BS alongside with number of users, we consider $C_{\text{HAP}}^{\max} = 5 \times 10^9$ cycles to be fixed, increase the available CPU in UAV-BSs, and plot the average AoI for different number of users in Fig. 4a. As we expected,

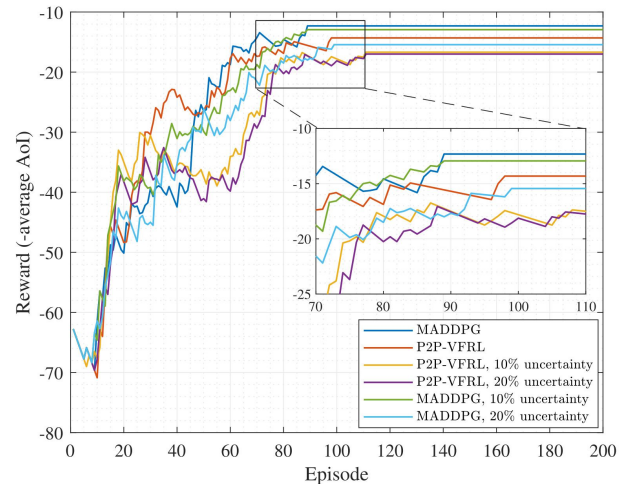


Fig. 3: Numerical assessment of reward of MADDPG and P2P-VFRL approaches over learning episodes.

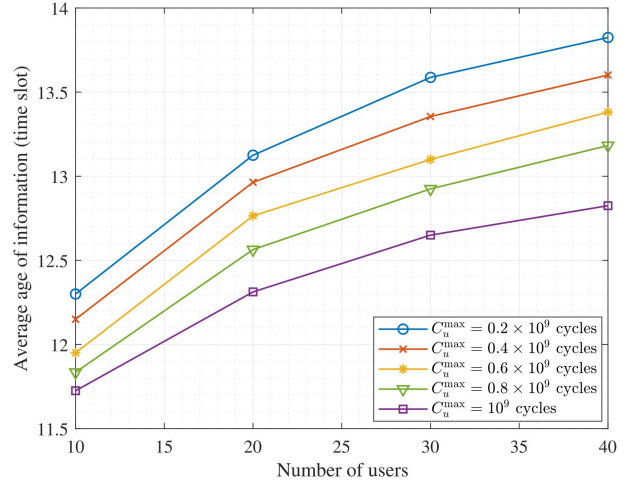
TABLE III: Average AoI improvement between MADDPG and baselines.

Baselines	average AoI gap
P2P-VFRL	-16%
MADDPG, 10% uncertainty	-5%
MADDPG, 20% uncertainty	-25%
P2P-VFRL, 10% uncertainty	-35%
P2P-VFRL, 20% uncertainty	-38%

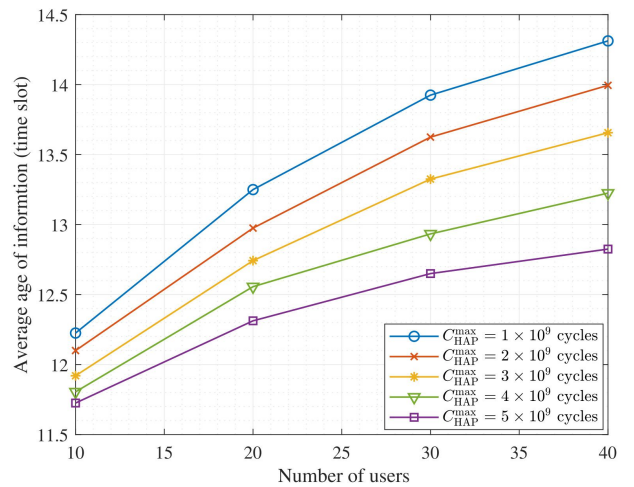
with higher amount of CPU power in UAV-BS, the tasks will be processed faster, leading to lower average AoI. Also, for analyzing the impact of available computing capacity in HAP, we consider $C_u^{\max} = 10^9$ cycles to be fixed, increase the available CPU power in the HAP, and plot the average AoI for different number of users in Fig. 4b, and a similar effect can be seen for the HAP computation capability on the average AoI. It is observed that the variation of HAP's computation capacity has a greater impact on the optimization results compared to the variation of UAV-BS's computation capacity. This is due to the fact that we assume the UAV-BS does not decide whether to allocate CPU for the remaining tasks in UAV-BS or to send them to the HAP in the next time slot. As a result, assigning more CPU resources to the HAP will result in lower average AoI.

2) *Maximum Transmission Power*: In this scenario, we analyze the impact of transmission power together with number of users on the average AoI and compare it with a baseline method, referred to as Baseline 1. In Baseline 1, tasks are sent without allocating transmission power but with their maximum power. As we can see in Fig. 5a, the AoI-based performance of NTN network improves by 9.98%, 9.92%, 10.86%, and 12.48%, for 10, 20, 30, and 40 users, respectively, and 10.81% in overall, in the case of increasing user's transmission power from 0.1 W to 0.2 W. Comparing with Baseline 1, for the mentioned number of users, it is shown that allocating power to users achieves a lower AoI. Moreover, it can be seen that with higher number of users, the difference between two modes increases which is due to the increase of interference in Baseline 1, which results in lower data rate and higher AoI, accordingly. For the UAV-BSs' transmission power, in Fig. 5b, the performance of the NTN network for 10, 20, 30, and 40 users improves by 8.22%, 8.32%, 11.20%, and 14.82%, respectively, and 10.64%, in overall, by allocating larger transmission power. Similar to the case of user's transmission power, allocation of power to UAV-BSs gets better results than Baseline 1, in which all UAV-BSs send users' tasks by their maximum power in each time slot for the mentioned number of users. In particular, we can observe that the average AoI decreases by increasing the transmission power of both users and UAV-BSs. Such trends are in accordance with formulas (4) and (7).

3) *Task size*: Another interesting scenario is changing the size of tasks. In order to see this scenario better, we compare it with another baseline method, considered by previous works [43], [44], referred to as Baseline 2. In this case, it is assumed that the tasks are not separable and must be sent in one time slot and the computing capacity for the whole task is allocated either in UAV-BS or HAP but not partially at both. In other



(a) Impact of UAV-BSs' computation capability ($C_{\text{HAP}}^{\max} = 5 \times 10^9$ cycles).



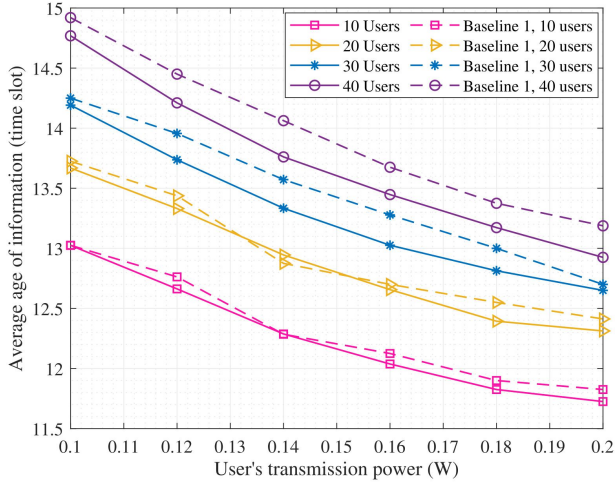
(b) Impact of HAP's computation capability ($C_u^{\max} = 10^9$ cycles).

Fig. 4: Impact of computation capability on network performance.

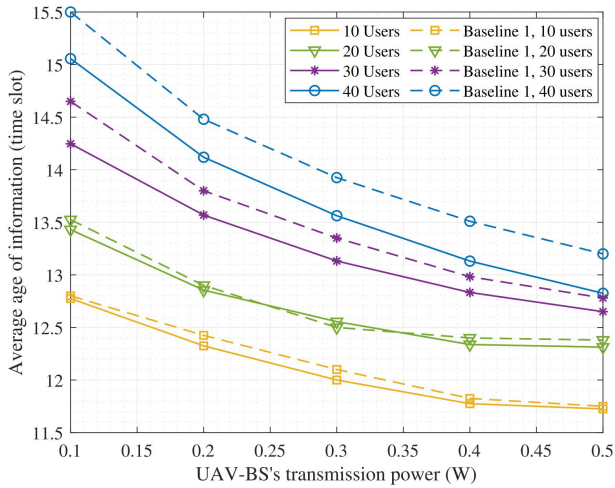
words, if the bandwidth and data rate assigned to the user is not sufficient to send a task, the task is not sent and the AoI increases, and also if the task reaches UAV-BS, but there is not enough capacity to process the entire task, AoI increases. Similarly, for sending data from UAV-BS to HAP, the same condition of sending and processing applies. Therefore, for this particular baseline scheme, we consider the following constraints:

$$\begin{aligned} \alpha_{m,s}(t), \beta_{m,s}^u(t) &= \{0, \alpha_{m,s}\}, \\ \eta_{m,s}(t), \theta_{m,s}^u(t) &= \{0, 1\}. \end{aligned} \quad (36)$$

This comparison is represented in Fig. 6. As expected, with the increase in the size of the task, the value of AoI also increases, and this effect is more profound for Baseline 2 scheme. This is such that for task sizes of 8×10^5 and 10^6 bits, the NTN network is not able to transmit at all which



(a) Impact of users' transmission power.



(b) Impact of UAV-BSs' transmission power.

Fig. 5: Impact of transmission power on network performance.

leads to AoI to become unacceptably large. This is referred to as transmission fail.

4) *Number of Subchannels*: Fig. 7 demonstrates the impact of the number of subchannels on the value of average AoI for different numbers of users. This figure shows that by increasing the number of subcarriers, and in other words, by increasing the bandwidth of each UAV-BS, more users send their tasks in each time slot, and as a result, more tasks are sent to the UAV-BS. The AoI-based performance for 10, 20, 30, and 40 users improved by 6.98%, 7.01%, 10.35%, and 11.98%, respectively. Nonetheless, as UAV-BSs are limited in their computation capacity, this parameter has a less profound effect on average AoI than the computing capacity of UAV-BS and HAP (Fig. 4), as the average AoI does not improve that much for a larger number of subchannels.

5) *CSI Uncertainty*: To have a comparison of the effect of CSI imperfectness, we examine the average AoI by increasing the CSI uncertainty bound value in a range of 0% to 20%. Channel gain has a direct impact on the data rate formula (4).

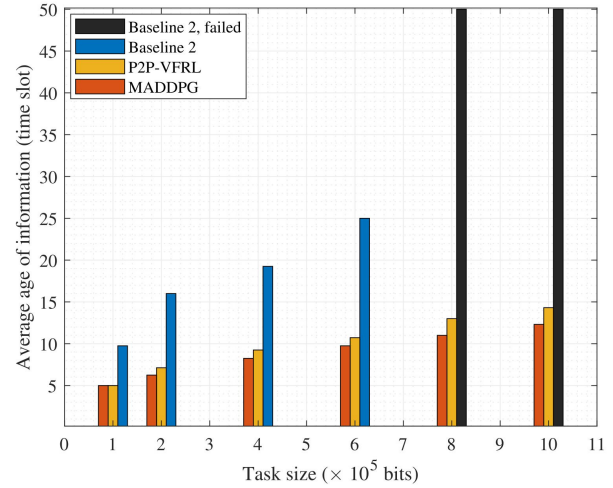


Fig. 6: Comparing our two methods to Baseline 2 for different task sizes.

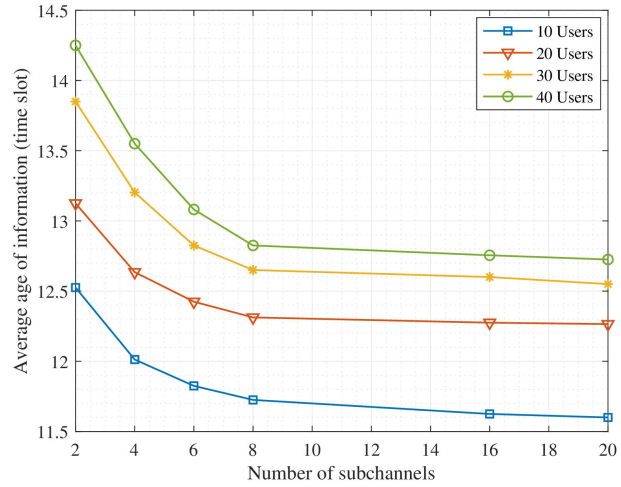


Fig. 7: Impact of number of subchannels on AoI-based NTN performance.

As the CSI uncertainty bound increases, the amount of data rate allocated to each user decreases at each time slot which leads to a decrease in the portion of the task that is sent. As in our system model, the AoI is inversely proportional to data rate, the average AoI increases, as depicted in Figs. 3 and 8.

6) *CSI Uncertainty*: To have a comparison of the effect of CSI imperfectness, we examine the average AoI by increasing the CSI uncertainty bound value in a range of 0% to 20%. Channel gain has a direct impact on the data rate formula (4). As the CSI uncertainty bound increases, the amount of data rate allocated to each user decreases at each time slot which leads to a decrease in the portion of the task that is sent. As in our system model, the AoI is inversely proportional to data rate, the average AoI increases, as depicted in Figs. 3 and 8.

7) *Trajectory*: To cover the mobile users in the area, UAV-BSs are also mobile. In Fig. 9, we considered an example which includes 2 UAV-BSs and 20 users and plot the corresponding trajectory for the UAV-BSs as well as the location

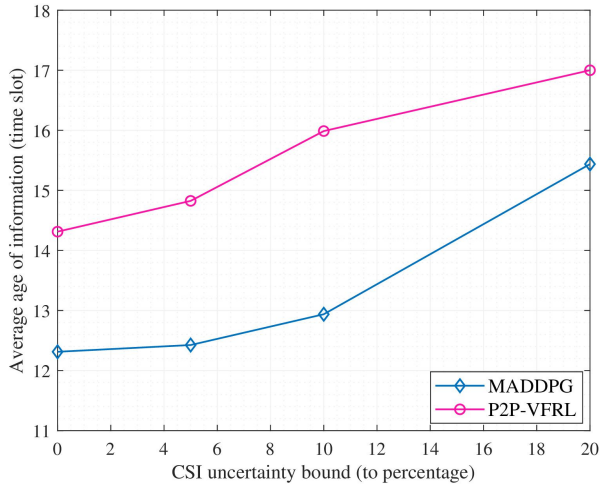


Fig. 8: Impact of uncertainty on network performance.

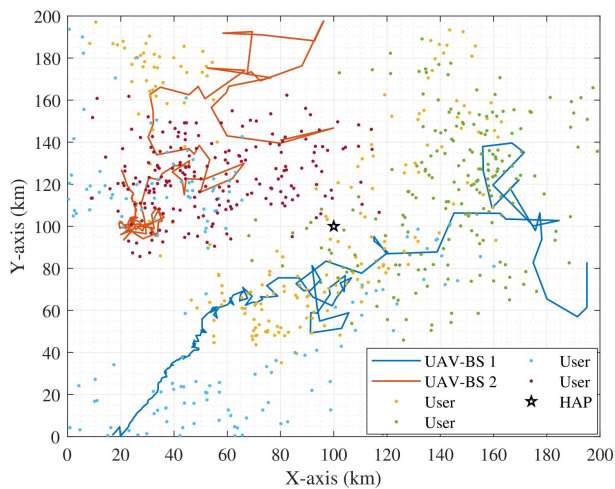


Fig. 9: Trajectory of UAV-BSs and users' movement.

of 4 of the users. We assume that the location of the HAP is fixed during operation time. As can be seen, the UAV-BSs move so as to provide proper coverage.

V. CONCLUSION

In this paper, we investigated the AoI sensitive two-tier aerial network including multiple UAV-BSs and a HAP, and provided online learning-based algorithms for channel, power, and computation capacity allocation and trajectory planning under CSI uncertainty in user-UAV-BS uplinks. The goal was to minimize the AoI of all users, who send their tasks to be processed. By adopting FL, and considering two types of agents in our environment, we developed a peer-to-peer online VFRL and compared it with well-known algorithm of MADDPG. We implemented a simulation setup with computationally-intensive applications. According to the results, for smaller task sizes, task scheduling reduces the average AoI approximately in half. For larger task size, the AoI gets unacceptably large if we rely on existing methods while

by deploying task scheduling, the AoI decreases significantly and to an acceptable level. On the other hand, power allocation for both users and UAV-BSs has a marginal effect on the average AoI compared to using full transmission power. As a future work, one can consider a case where the UAV-BSs' selection ability is extended. For example, they can decide whether the remaining tasks in a UAV-BS have to be processed or sent to the HAP in the next time slot. In addition, choosing the optimized weights of the actor network parameters at each training step of P2P-VFRL algorithm can be considered as an action which may bring better results to reduce the performance gap between MADDPG and P2P-VFRL approaches.

REFERENCES

- [1] "Study on support of reduced capability NR devices (Release 17)," TR 38.875, 3rd Generation Partnership Project (3GPP), 2020.
- [2] "Redcap - expanding the 5g device ecosystem for consumers and industries." Ericsson Whitepaper, 2023.
- [3] G. K. Kurt, M. G. Khoshkholgh, S. Alfattani, A. Ibrahim, T. S. Darwish, M. S. Alam, H. Yanikomeroglu, and A. Yongacoglu, "A vision and framework for the high altitude platform station (HAPS) networks of the future," *IEEE Communications Surveys & Tutorials*, vol. 23, no. 2, pp. 729–779, 2021.
- [4] R. Austin, *Unmanned aircraft systems: UAVS design, development and deployment*, vol. 54. John Wiley & Sons, 2011.
- [5] R. W. Beard and T. W. McLain, *Small unmanned aircraft: Theory and practice*. Princeton university press, 2012.
- [6] Q. Wu, Y. Zeng, and R. Zhang, "Joint trajectory and communication design for multi-UAV enabled wireless networks," *IEEE Transactions on Wireless Communications*, vol. 17, no. 3, pp. 2109–2121, 2018.
- [7] C. Zhan, Y. Zeng, and R. Zhang, "Energy-efficient data collection in UAV enabled wireless sensor network," *IEEE Wireless Communications Letters*, vol. 7, no. 3, pp. 328–331, 2017.
- [8] S. Kaul, R. Yates, and M. Gruteser, "Real-time status: How often should one update?," in *2012 Proceedings IEEE INFOCOM*, pp. 2731–2735, IEEE, 2012.
- [9] C. Kam, S. Kompella, and A. Ephremides, "Age of information under random updates," in *2013 IEEE International Symposium on Information Theory*, pp. 66–70, IEEE, 2013.
- [10] Y. Sun, E. Uysal-Biyikoglu, R. D. Yates, C. E. Koksall, and N. B. Shroff, "Update or wait: How to keep your data fresh," *IEEE Transactions on Information Theory*, vol. 63, no. 11, pp. 7492–7508, 2017.
- [11] C. Shen, T.-H. Chang, K.-Y. Wang, Z. Qiu, and C.-Y. Chi, "Distributed robust multicell coordinated beamforming with imperfect CSI: An ADMM approach," *IEEE Transactions on signal processing*, vol. 60, no. 6, pp. 2988–3003, 2012.
- [12] T. Naous, M. Itani, M. Awad, and S. Sharafeddine, "Reinforcement learning in the sky: A survey on enabling intelligence in ntn-based communications," *IEEE Access*, 2023.
- [13] R. Lowe, Y. Wu, A. Tamar, J. Harb, P. Abbeel, and I. Mordatch, "Multi-agent actor-critic for mixed cooperative-competitive environments," *arXiv preprint arXiv:1706.02275*, 2017.
- [14] P. K. Sharma and D. I. Kim, "UAV-enabled downlink wireless system with non-orthogonal multiple access," in *2017 IEEE Globecom Workshops (GC Wkshps)*, pp. 1–6, IEEE, 2017.
- [15] M. F. Sohail, C. Y. Leow, and S. Won, "Non-orthogonal multiple access for unmanned aerial vehicle assisted communication," *IEEE Access*, vol. 6, pp. 22716–22727, 2018.
- [16] T. Hou, Y. Liu, Z. Song, X. Sun, and Y. Chen, "Multiple antenna aided NOMA in UAV networks: A stochastic geometry approach," *IEEE Transactions on Communications*, vol. 67, no. 2, pp. 1031–1044, 2018.
- [17] W. Fan, K. Luo, S. Yu, Z. Zhou, and X. Chen, "AoI-driven fresh situation awareness by UAV swarm: Collaborative DRL-based energy-efficient trajectory control and data processing," in *2020 IEEE/CIC International Conference on Communications in China (ICCC)*, pp. 841–846, IEEE, 2020.
- [18] Z. Yang, C. Pan, K. Wang, and M. Shikh-Bahaei, "Energy efficient resource allocation in UAV-enabled mobile edge computing networks," *IEEE Transactions on Wireless Communications*, vol. 18, no. 9, pp. 4576–4589, 2019.

- [19] B. Yang, X. Cao, C. Yuen, and L. Qian, "Offloading optimization in edge computing for deep-learning-enabled target tracking by internet of UAVs," *IEEE Internet of Things Journal*, vol. 8, no. 12, pp. 9878–9893, 2020.
- [20] S. Wang, M. Chen, C. Yin, W. Saad, C. S. Hong, S. Cui, and H. V. Poor, "Federated learning for task and resource allocation in wireless high-altitude balloon networks," *IEEE Internet of Things Journal*, vol. 8, no. 24, pp. 17460–17475, 2021.
- [21] Z. Jia, Q. Wu, C. Dong, C. Yuen, and Z. Han, "Hierarchical aerial computing for internet of things via cooperation of HAPs and UAVs," *IEEE Internet of Things Journal*, 2022.
- [22] Y. Peng, Y. Liu, D. Li, and H. Zhang, "Deep reinforcement learning based freshness-aware path planning for UAV-assisted edge computing networks with device mobility," *Remote Sensing*, vol. 14, no. 16, p. 4016, 2022.
- [23] Z. Jia, X. Qin, Z. Wang, and B. Liu, "Age-based path planning and data acquisition in UAV-assisted IoT networks," in 2019 IEEE International Conference on Communications Workshops (ICC Workshops), pp. 1–6, IEEE, 2019.
- [24] J. Liu, X. Wang, B. Bai, and H. Dai, "Age-optimal trajectory planning for UAV-assisted data collection," in IEEE INFOCOM 2018-IEEE Conference on Computer Communications Workshops (INFOCOM WKSHPs), pp. 553–558, IEEE, 2018.
- [25] P. Tong, J. Liu, X. Wang, B. Bai, and H. Dai, "UAV-enabled age-optimal data collection in wireless sensor networks," in 2019 IEEE International Conference on Communications Workshops (ICC Workshops), pp. 1–6, IEEE, 2019.
- [26] X. Wang, Z. Ning, and S. Guo, "Multi-agent imitation learning for pervasive edge computing: A decentralized computation offloading algorithm," *IEEE Transactions on Parallel and Distributed Systems*, vol. 32, no. 2, pp. 411–425, 2020.
- [27] H. Hu, K. Xiong, G. Qu, Q. Ni, P. Fan, and K. B. Letaief, "AoI-minimal trajectory planning and data collection in UAV-assisted wireless powered IoT networks," *IEEE Internet of Things Journal*, vol. 8, no. 2, pp. 1211–1223, 2020.
- [28] H. xia Peng and X. Shen, "Multi-agent reinforcement learning based resource management in MEC- and UAV-assisted vehicular networks," *IEEE Journal on Selected Areas in Communications*, vol. 39, pp. 131–141, 2021.
- [29] Z. Zhu, S. Wan, P. Fan, and K. B. Letaief, "Federated multiagent actor-critic learning for age sensitive mobile-edge computing," *IEEE Internet of Things Journal*, vol. 9, no. 2, pp. 1053–1067, 2021.
- [30] C. Tin, *Robust multi-UAV planning in dynamic and uncertain environments*. PhD thesis, Massachusetts Institute of Technology, 2004.
- [31] S. Farazi, A. G. Klein, and D. R. Brown, "On the average staleness of global channel state information in wireless networks with random transmit node selection," in 2016 IEEE International Conference on Acoustics, Speech and Signal Processing (ICASSP), pp. 3621–3625, IEEE, 2016.
- [32] M. S. Ali, H. Tabassum, and E. Hossain, "Dynamic user clustering and power allocation for uplink and downlink non-orthogonal multiple access (NOMA) systems," *IEEE access*, vol. 4, pp. 6325–6343, 2016.
- [33] Y. Yuan and Z. Ding, "Outage constrained secrecy rate maximization design with SWIPT in MIMO-CR systems," *IEEE Transactions on Vehicular Technology*, vol. 67, no. 6, pp. 5475–5480, 2017.
- [34] Y. Xu, G. Li, Y. Yang, M. Liu, and G. Gui, "Robust resource allocation and power splitting in SWIPT enabled heterogeneous networks: A robust minimax approach," *IEEE Internet of Things Journal*, vol. 6, no. 6, pp. 10799–10811, 2019.
- [35] F. Zhou, Z. Li, J. Cheng, Q. Li, and J. Si, "Robust AN-aided beamforming and power splitting design for secure MISO cognitive radio with SWIPT," *IEEE Transactions on Wireless Communications*, vol. 16, no. 4, pp. 2450–2464, 2017.
- [36] L. Zhang, G. Zhao, W. Zhou, L. Li, G. Wu, Y.-C. Liang, and S. Li, "Primary channel gain estimation for spectrum sharing in cognitive radio networks," *IEEE transactions on communications*, vol. 65, no. 10, pp. 4152–4162, 2017.
- [37] T. P. Lillicrap, J. J. Hunt, A. Pritzel, N. Heess, T. Erez, Y. Tassa, D. Silver, and D. Wierstra, "Continuous control with deep reinforcement learning," *arXiv preprint arXiv:1509.02971*, 2015.
- [38] J. Qi, Q. Zhou, L. Lei, and K. Zheng, "Federated reinforcement learning: techniques, applications, and open challenges," *arXiv preprint arXiv:2108.11887*, 2021.
- [39] D. Mäenpää, "Towards peer-to-peer federated learning: Algorithms and comparisons to centralized federated learning," 2021.
- [40] H. Dong, Z. Ding, S. Zhang, and Chang, *Deep Reinforcement Learning*. Springer, 2020.
- [41] B. McMahan, E. Moore, D. Ramage, S. Hampson, and B. A. y Arcas, "Communication-efficient learning of deep networks from decentralized data," in Artificial intelligence and statistics, pp. 1273–1282, PMLR, 2017.
- [42] M. Ansarifard, "MADDPG and P2P-VFRL for minimizing AoI in NTN network under CSI uncertainty." <https://dx.doi.org/10.21227/8yvb-e654>, 2022.
- [43] R. V. Bhat, R. Vaze, and M. Motani, "Throughput maximization with an average age of information constraint in fading channels," *IEEE Transactions on Wireless Communications*, vol. 20, no. 1, pp. 481–494, 2020.
- [44] M. Moltafet, M. Leinonen, M. Codreanu, and N. Pappas, "Power minimization in wireless sensor networks with constrained AoI using stochastic optimization," in 2019 53rd Asilomar Conference on Signals, Systems, and Computers, pp. 406–410, IEEE, 2019.